ACS Catalysis
Research Article
pubs.acs.org/acscatalysis

NbF_5−AlF_3 Catalysts: Design, Synthesis, and Application in Lactic Acid Synthesis from Cellulose

Simona M. Coman,*,† Marian Verziu,† Alina Tirsoaga,‡ Bogdan Jurca,‡ Cristian Teodorescu,§ Victor Kuncser,§ Vasile I. Parvulescu,*,† Gudrun Scholz,∥ and Erhard Kemnitz*,∥

†Department of Organic Chemistry, Biochemistry and Catalysis and ‡Department of Physical Chemistry, Faculty of Chemistry, University of Bucharest, Bdul Regina Elisabeta, 4-12, Bucharest 030016, Romania

§National Institute of Materials Physics, Atomistilor 105b, 077125 Magurele-Ilfov, Romania

∥Department of Chemistry, Humboldt-Universität zu Berlin, Brook-Taylor-Straße 2, D-12489 Berlin, Germany

Supporting Information

ABSTRACT: A series of niobium-modified aluminum hydroxide fluorides (denoted Nb@AlF_3), prepared via a fluorolytic sol−gel synthesis was investigated for the catalytic one-pot conversion of cellulose to lactic acid. The structure of the new acid catalysts is the result of the dispersion of niobium fluoride in an aluminum hydroxide fluoride matrix. The calcination of the catalysts at a relatively low temperature (350 °C) stabilized this structure. Catalytic performances in terms of lactic acid yields are directly correlated with the niobium content.

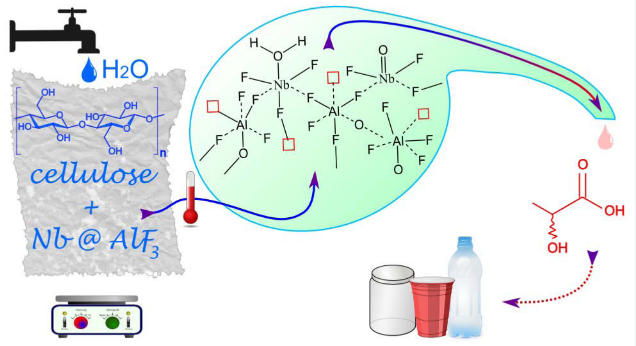

KEYWORDS: *niobium fluoride, aluminum fluoride, acidity, cellulose, lactic acid*

1. INTRODUCTION

In direct relation with the depletion of petroleum and the serious environmental pollution caused by the utilization of fossil resources, in the last few years, both academia and industry have focused their attention toward biorefinery. In this context the production of chemicals from renewable resources appears to be even more important than that of biofuels.[1] Cellulose has become an important target, and the identification of selective catalysts for its transformation toward value-added products is of major industrial importance.[2] However, the production of biochemicals or biofuels from cellulose is not an easy task, due to its robust crystalline structure, which makes it an insoluble compound in most organic solvents.[3] This property complicates the use of solid catalysts, and thereby, the discovery and investigation of novel and efficient pathways as well as catalysts for the conversion of cellulose into chemicals are great challenges facing heterogeneous catalysis. However, although the research in this field is very intense and novel transformation routes/catalytic materials have been discovered at a high rate, the specific properties of cellulose still impose new requirements.

Lactic acid, one of the most important platform molecules obtained from biomass, is currently used in the food, cosmetic, pharmaceutical, and chemical industries (e.g., the synthesis of alkyl lactates, which can be used as environmentally benign solvents[4]), but its polymerization to poly(lactic) acid, a biodegradable polymer, is another promising and rapidly growing application.[4−8] It may also find applications in a much wider range of industries than is the case today for the polymer industry (through its dehydration to acrylic acid, an industrially important monomer)[9] and in domestic areas (the production of propylene glycol, a nontoxic antifreeze[6]). For the moment its current relatively high price precludes many of the applications listed above, being produced almost exclusively through the fermentation of sugars. The process takes place with a low volumetric production rate, requires alkaline salt addition to maintain the pH of the fermentation broth, and is accompanied by the concomitant generation of significant amounts of wastes.[8] In this context, wider adoption would be reliant on the identification of more efficient and less costly production methods in comparison to the current fermentation procedure.

The use of heterogeneous catalysis would, therefore, be an attractive method if it can be developed as a more efficient process. Several catalytic processes alternative to fermentative methods have been developed already, but they still need improvements to become competitive on the industrial level. The alkaline degradation of carbohydrates for producing lactic acid has been reported, but the process takes place with quite low selectivity.[10] Another option is the selective oxidation of

Received: February 10, 2015
Revised: April 6, 2015
Published: April 8, 2015

DOI: 10.1021/acscatal.5b00282
ACS Catal. 2015, 5, 3013−3026

1,2-propanediol (obtained by the dehydration of glycerol) in the presence of gold-based nanoparticulate catalysts and inorganic bases.[11] Although it is more environmentally benign than the alkaline degradation of carbohydrates, this method still has some difficulties such as workup under high pressure and the use of inorganic bases, which are at odds with the principles of green chemistry. Therefore, a more promising method for the lactic acid derivative synthesis seems to be the Lewis acid catalyzed isomerization/esterification of triose sugars, reported by different authors.[12−16] In this respect, an even more interesting method appears to be the use of hexose sugars as raw materials and stannosilicates as catalysts. This route may generate methyl lactate and has the advantage of lower cost of the hexose sugars.[17,18] Even more, exploitation of heterogeneous catalyst processes directly leading to lactic acid from polysaccharides, such as cellulose, is highly demanded.

In recent years, niobia as well as modified niobia have been the focus of intense research, in a variety of important acid-catalyzed reactions in which water molecules are involved as a reactant or as a reaction product (e.g., dehydration, hydration, etherification, hydrolysis, condensation, dehydrogenation, alkylation, photochemical and electrochemical polymerization, and oxidation).[19−22] One of the reasons for this intense research is its remarkably high acidity ($H_o = -8.2$), which is also maintained in water.[23] Its behavior is also valuable to carry out deoxygenation of biomass derivatives in the aqueous phase through dehydration reactions.[24] However, commercial bulk niobia suffers from poor hydrothermal stability, resulting in a low surface area after use (and, consequently, low catalytic stability) in a high-water environment when the temperature is higher than 200 °C.[25,26] The deposition of niobia on oxide supports (silica, titania, alumina) somewhat improves the hydrothermal stability in aqueous-phase reactions.[27,28] Interestingly enough, the use of mixed oxides containing niobium or the deposition of niobia on various oxides leads to an enhancement of the acidity.[19,29] Lewis acidity was found in all of the supported niobium oxide systems, while Brønsted acid sites were only detected in niobium supported on alumina and silica.

The enhancement of Lewis acidity by aliovalent cation doping is well known for oxides and was extensively explored by Tanabe[30] and extended by Kemnitz to fluorides.[31] However, overly strong Lewis acids are not stable in the presence of moisture, making them unsuitable for many fine chemical productions which involve water as reactant, product, or reaction solvent. Therefore, to overcome the problems associated with the instability of strong Lewis acids, novel doped hydroxylated fluorides have been synthesized. In this context, not long ago a Sn-containing hydroxylated MgF_2 catalyst was successfully applied to the selective cellulose hydrolysis to glucose, in aqueous solution.[32]

Herein we will show that the hydroxylated fluoride concept can be successfully extended to niobium, resulting in materials such as Nb-containing hydroxylated AlF_3, with unexpected catalytic properties and improved stability against water. In an unprecedented way, in the presence of Nb-containing hydroxylated AlF_3 catalysts, the degradation of cellulose led not to glucose, as in the case of Sn-modified hydroxylated MgF_2, but to α-hydroxy acids (AHAs) as the main products, preponderantly lactic acid. In other words, the ability of niobium to catalyze a range of different reactions (as previously shown in the literature) combined with its stability against water has allowed the development of a cascade reaction, converting cellulose into α-hydroxy acids (AHAs) in a single reactor with a high yield.

2. EXPERIMENTAL SECTION

2.1. Catalyst Preparation. A series of nanoscopic Nb-containing aluminum fluorides with 10 and 25 mol % Nb, respectively, were synthesized through a fluorolytic sol−gel route as follows: $Al(O^iPr)_3$ and 25 mol % of $Nb(OEt)_5$ were dissolved in ethanol in a 3/1 Al/Nb molar ratio. To this solution was added anhydrous hydrogen fluoride (HF) in ethanol in a stoichiometric amount with regard to the overall metal equivalents added. Since the niobium precursor was in the oxidation state 5+, we used 3 equiv of HF for each Al^{3+} and 5 equiv of HF for each Nb^{5+}. The overall final concentration of the ultimately obtained ternary metal fluoride sols was 0.4 M with regard to the sum of n_{Al} and n_{Nb}, irrespective of their oxidation state. After this sol was stirred overnight, the solvent was removed under vacuum at 80 °C. Part of each prepared catalyst was forward calcined at 350 and 500 °C, respectively (5 °C/min, 24 h) in air. The obtained samples were denoted xNb@AlF_3-y, where x is the mole percent of Nb (10 and 25 mol % of Nb, respectively) and y = calcination temperature (e.g., 350 or 500 °C). For comparison hydroxylated aluminum fluoride, denoted as AlF_3-50, was also prepared following a previously reported procedure.[33]

2.2. Catalyst Characterization. The obtained catalysts were exhaustively characterized using different techniques such as adsorption−desorption isotherms of nitrogen at −196 °C (see the Supporting Information), powder X-ray diffraction (XRD) (see the Supporting Information), Raman spectroscopy (see the Supporting Information), X-ray photoelectron spectrometry (XPS), ICP-OES, magnetic measurements, ^{19}F and ^{27}Al MAS NMR, diffuse reflectance infrared Fourier transform spectroscopy (DRIFT), and infrared photoacoustic spectroscopy of chemisorbed pyridine (Py-IR).

XPS measurements were performed at normal emission in a Specs setup, by using Al Kα monochromated radiation ($h\nu$ = 1486.7 eV) from an X-ray gun, operating at 300 W (12 kV/25 mA) power. A flood gun with electron acceleration at 1 eV and electron current of 100 μA was used in order to avoid charge effects. Photoelectron energy was recorded in normal emission by using a Phoibos 150 analyzer, operating with a pass energy of 30 eV. The XPS spectra were fitted by using Voigt profiles combined with their primitive functions, for inelastic backgrounds.[34] The Gaussian widths of all lines and thresholds are the same for one spectrum and do not differ considerably from one spectrum to another, always being in the range of 2 eV. For doublets, the resulting branching ratios did not differ significantly from their theoretical value (1.5 for Nb 3d, 2 for Al 2p).

The contents of niobium and aluminum were determined by ICP-OES (Agilent Technologies, 700 Series) after calibrating the instrument with standard solutions. The amount of fluoride in the samples was determined by the Seel method, under the same conditions as described previously.[35]

Magnetic hysteresis loops at different temperatures and thermomagnetic curves in the temperature range from 5 to 300 K were measured with a SQUID magnetometer (MPMS Quantum Design) by using the most sensitive RS (reciprocal space) option.

Both ^{19}F and ^{27}Al MAS NMR spectra were recorded on a Bruker Avance 400 spectrometer in a 2.5 mm MAS probe with 2.5 mm rotors made from ZrO_2. A rotation frequency of 20 kHz was applied. The ^{19}F MAS NMR spectra were recorded with a $\pi/2$ pulse duration of 3.3 μs, a spectrum width of 400 kHz, a recycle delay of 5 s, and accumulation numbers between 64 and 512. The isotropic chemical shifts δ_{iso} of ^{19}F resonances are given relative to $CFCl_3$ standard using α-AlF_3 as secondary standard ($\delta_{^{19}F}$ −172.6 ppm). Existent background signals of ^{19}F were suppressed with the application of a phase-cycled depth pulse sequence according to Cory et al.[36]

^{27}Al MAS NMR ($I = 5/2$) spectra were recorded with an excitation pulse duration of 1 μs. A 1 M aqueous solution of $AlCl_3$ was used as reference for the chemical shift of ^{27}Al. The recycle delay was chosen as 1 s, and accumulation numbers up to 2048 were taken.

DRIFT spectra were recorded using a Thermo Electron Nicolet 4700 FTIR spectrometer with a Smart Accessory for diffuse reflectance measurements, in a gastight in situ cell. The IR spectra were scanned in the region of 4000−400 cm^{-1}. The final spectra are an accumulation of 400 scans. All spectra were recorded under a nitrogen flow in order to ensure the evacuation of desorbed species. The baseline was collected using KBr as reference, which was kept 10 min under the nitrogen flow before recording. The analyzed sample was kept 15 min under nitrogen before recording the spectra at room temperature, and then the in situ chamber was heated to 150 °C and kept another 15 min before the recording of the spectrum.

Infrared photoacoustic spectroscopy of chemisorbed pyridine was employed for the determination of the nature of acid sites (Lewis/Brønsted) on the catalyst surfaces. A 30 μL portion of liquid pyridine was injected into a vaporizer (located on the inlet of the reactor, permanent nitrogen flow) and passed to the solid sample pressed into a self-supporting pellet (2 cm^2, 70 mg, pressure of 1.5 tons) at 150 °C in a flow system. The excess gaseous and physisorbed pyridine was removed by purging with dried nitrogen. After it was cooled to room temperature, the sample was transferred into an MTECH photoacoustic cell coupled with a FTIR spectrometer. The whole procedure was carried out under the same conditions as described previously.[37]

2.3. Catalytic Reaction. α-Cellulose (purchased from Sigma-Aldrich, product no. C8002) contained 92.2% glucan and 7.8% xylan, on a dry basis, in accordance with the previous analysis performed by Torget and co-workers[38] and a broad distribution of the polymerization degree (PD) with a maximum value of 1.5×10^3, determined by gel permeation chromatography of the tricarbanilate derivative of the cellulose sample, in agreement with previous studies of Schüth et al.[39]

Activity tests in batch mode were carried out in a stainless-steel autoclave (Parr) by the following procedure: to a slurry of 0.16 or 0.56 g of α-cellulose in 5 or 30 mL of water was added 0.06 or 0.056 g of xNb@AlF_{3}-y catalyst and the mixture was heated to 150−180 °C, with stirring (1200 rpm), for 2−48 h. After the reaction the catalyst and untransformed cellulose were filtered off from the slurry of products and the water-soluble products were separated by distillation under vacuum. The recovered products were silylated, diluted with 1 mL of toluene, and analyzed by GC-FID chromatography (GC-Shimadzu apparatus). The identification of the products was carried out using a GC-MS Carlo Erba Instruments QMD 1000 equipped with a Factor Four VF-5HT column. The fragmentation pathways of the products are described in detail in Scheme S1 and Figure S7 of the Supporting Information.

The conversion of cellulose (X) was determined on the basis of the weight of cellulose introduced into the reaction mixture ($m_{\mathrm{cellulose,0}}$) and of the solid recovered after reaction with the consideration of the solid catalyst: $m_{\mathrm{Cellulose}} = m_{\mathrm{recovered\ solid}} - m_{\mathrm{Catalyst}}$

$$X = \frac{m_{\mathrm{cellulose,0}} - m_{\mathrm{cellulose}}}{m_{\mathrm{cellulose,0}}} \tag{1}$$

On the basis of the conversion of cellulose and the yield of products in the liquid phase (Y_{liquid}), identified by GC-FID chromatography, an overall selectivity to liquid-phase products, expressed as carbon efficiency (E_C), may be calculated as

$$E_C = \frac{Y_{\mathrm{liquid}}}{X} \times 100 \tag{2}$$

Finally, the selectivity to each product in the liquid phase was calculated on the basis of eq 3.

$$S\ (\%) = \frac{Y_i}{Y_{\mathrm{liquid}}} \times 100 \tag{3}$$

For catalytic leaching the following test was made: 0.06 g of 25Nb@AlF_3 (no calcination) was boiled in 5 mL of water, at 180 °C, for 2 h, with stirring. After 2 h, the catalyst was separated from the liquid medium by centrifugation. In the liquid phase (with a light yellow color) 0.16 g of cellulose was added and kept at 180 °C for 2 h, with stirring. The separated solid catalyst was washed and dried at room temperature and then used in the reaction test under the following conditions: 0.16 g of cellulose, 5 mL of water, 180 °C, and 2 h reaction time.

To investigate the chemical stability of the catalysts, the content of the leached metal into the reaction liquid was determined by ICP-OES (Agilent Technologies, 700 Series), while the leached organic species were detected by electrical conductivity measurements of a catalyst/water slurry, at room temperature (see the Supporting Information).

3. RESULTS AND DISCUSSION

Due to the high structural distortion that has been introduced by the synthesis procedure employed, phase analysis based on in situ collected X-ray diffraction (XRD) patterns of the Nb-doped hydroxylated fluorides at different temperatures is less informative. Nevertheless, the XRD analysis of the ex situ calcined samples at 500 °C indicates the coexistence of niobium oxide fluorides very rich in oxygen ($Nb_{31}O_{77}F$: JCPDS 19-0865) and mixed Al−Nb−O_x oxides (see Figures S1 and S2 in the Supporting Information). However, ^{27}Al and ^{19}F are very suitable nuclei to monitor local structures present in the samples by solid-state NMR spectroscopy.

Both ^{27}Al and ^{19}F MAS NMR spectra of the catalyst are shown in Figure 1 for 10Nb@AlF_3 and Figure 2 for 25Nb@AlF_3. The chemical shift values of the maxima of the signals are given directly in the figures. The samples obtained after the sol−gel synthesis and used for the studies without further calcination show in both cases the typical ^{27}Al and ^{19}F signals for an AlF_3 matrix with partial oxygen content. Aluminum exists exclusively in 6-fold coordination, and from the chemical shift values we know that the average coordination for aluminum is AlF_5O.[40−42]

A thermal treatment in air, however, distinctly changes local coordinations. In addition to the still present 6-fold coordinated Al units AlF_xO_{6-x} (x = 5, 6), the ^{27}Al MAS NMR spectra give

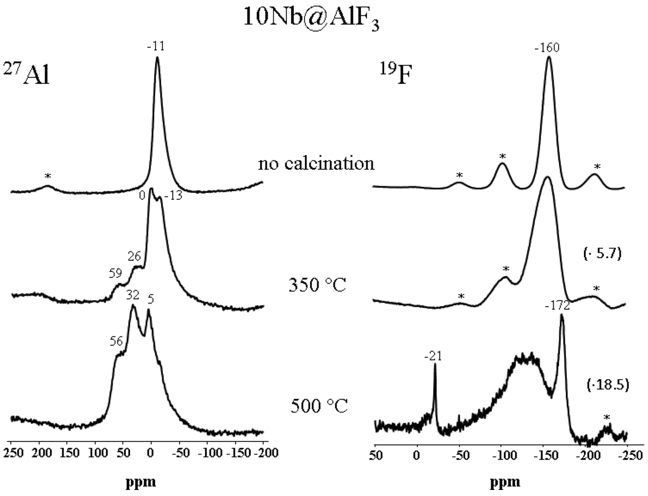

Figure 1. ^{27}Al and ^{19}F MAS NMR spectra of the 10Nb@AlF$_3$ catalysts.

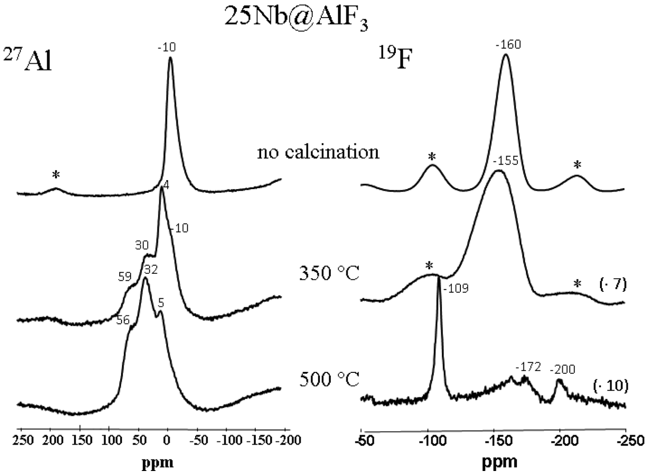

Figure 2. ^{27}Al and ^{19}F MAS NMR spectra of the 25Nb@AlF$_3$ catalysts.

clear evidence for the formation of additional, different AlF$_x$O$_{6-x}$ units with higher oxygen content (x = 0, 1; chemical shift at 0–4 ppm), 5-fold coordinated units AlF$_x$O$_{5-x}$ (chemical shift values between 26 and 32 ppm), and 4-fold coordinated species AlF$_x$O$_{4-x}$ (signals at about 56–59 ppm). These findings are in agreement with the ^{19}F MAS NMR spectra, which result in an asymmetric line broadening into the low-field direction. The formation of presumably mainly oxygen coordinated 4-, 5- and 6-fold coordinated Al units in both samples is more pronounced after calcination at 500 °C. The number of predominantly fluorine coordinated Al sites is drastically reduced. Strong support comes from the ^{19}F MAS NMR spectra showing a substantial fluorine loss under these preparation conditions. This effect is a consequence of beginning AlF$_3$ sublimation and local reactions due to pyrohydrolysis.[43] Thus, it was evidenced that calcination of nanoscopic AlF$_3$ that has not been sufficiently dried results already partially in hydrolysis, thus forming AlOF moieties. The extent of the pyrohydrolysis increases with increasing moisture content of the air used, as has been evidenced in ref 43. The ^{19}F spectra given in Figures 1 and 2 had to be enlarged by the factors directly given in the figures. Whereas residues of AlF$_6$ species are still present (−172 ppm), most of the intensity of fluorine signals disappeared and new signals at −21 ppm (10Nb@AlF$_3$) and −109 ppm (25Nb@AlF$_3$) can now be detected. These fluorine signals point to the formation of NbO$_x$F$_y$ species, which is in agreement with findings in the literature[44,45] and XRD analysis (see Figures S1 and S2 in the Supporting Information).

XPS Al(2p) spectra for dried and calcined 10Nb@AlF$_3$ and 25Nb@AlF$_3$ samples are illustrated in Figure 3. Depending on the catalysts treatment, the deconvoluted Al(2p) spectra indicate the presence of different Al sites with binding energies at different BE positions (Table 1). For the noncalcined samples, the deconvoluted spectrum is composed of three peaks located at around 76.4, 74.5–75.1, and 72.5–73.1 eV, respectively. They can be explained by the occurrence of differently coordinated Al sites. Thus, the bands at 76.4 eV

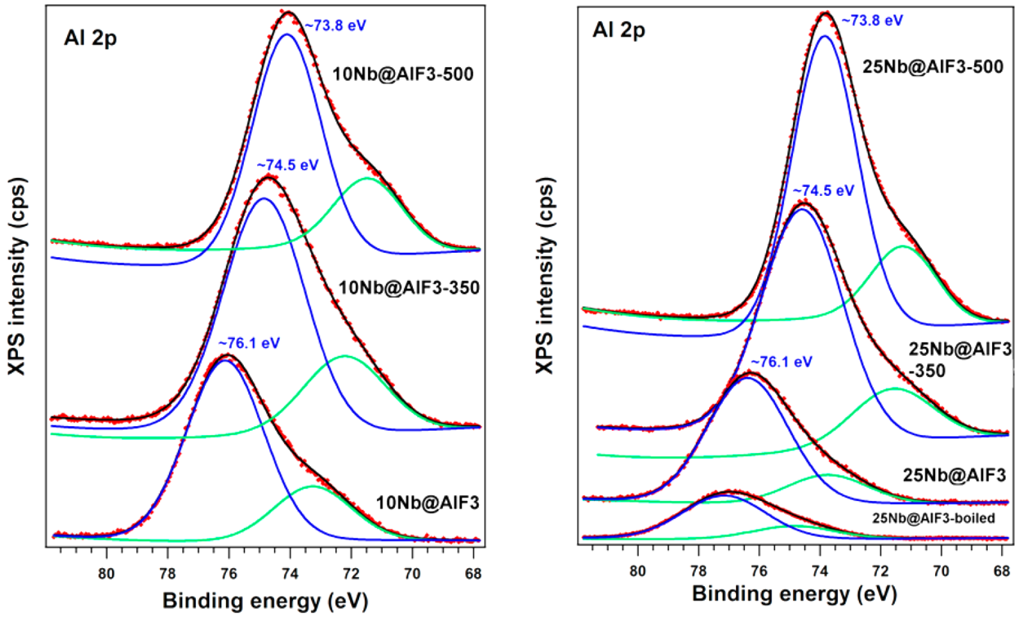

Figure 3. XP spectra of the Al (2p) level for the 10Nb@AlF$_3$ and 25Nb@AlF$_3$ samples.

DOI: 10.1021/acscatal.5b00282
ACS Catal. 2015, 5, 3013–3026

Table 1. Binding Energy of the Al_{2p} Level as a Function of the Treatment Conditions

	binding energy of Al_{2p} level (eV)					
sample	C1	C2	C3	C4	C5	C6
10Nb@AlF_3	76.3	74.5		72.5		
10Nb@AlF_3-350	76.4	74.9	73.4		71.6	
10Nb@AlF_3-500		74.2		72.7		70.9
25Nb@AlF_3	76.5	75.1		73.1		
25Nb@AlF_3-350	75.7	74.5		72.7		70.9
25Nb@AlF_3-500			73.9	72.3		70.6

could be assigned to aluminum in AlF_3,[46] that around 75 eV to aluminum inserted in framework porous structures such as molecular sieves,[47,48] which in our case is rather due to a high degree of structural distortion, and that at around 73 eV to aluminum in alumina.[49−51]

Increasing the calcination temperature causes a change in the coordination of aluminum. Thus, after calcination at 350 °C the band assigned to AlF_3 suffered an important decrease, while after calcination at 500 °C the band almost completely vanished (Figure 3). In addition, the calcination temperature led in a first instance (350 °C) to an increase in the intensity of the band assigned to aluminum inserted in a highly distorted framework-like porous $AlF_{3-x}(OH)_x$ phase and also in that of alumina. Finally, calcination at 500 °C led to a shift of BE levels of the bands assigned to aluminum in alumina that is typical for the transformation in more ordered alumina structures (Figure 3).[50]

XPS spectra for a noncalcined 25Nb@AlF_3, after boiling in water, showed a BE level of Al(2p) centered at 76.9 eV. Such a value may indicate a "cleaning" of the surface by hydrolysis of the nonhydrolyzed −OiPr, which is less electronegative than F and the thus formed OH^- and/or O^{2-} ions, respectively.[52] This statement is in agreement with the XRD diffraction, which shows that the hydrothermal treatment prevents the high-temperature water loss (as observed in the calcined samples), thus preserving the chemical composition $Al_2[(OH)_{0.5}F_{0.5}]_6$ of the main crystalline phase from the noncalcined 25Nb@AlF_3 sample (Figure S3 in the Supporting Information), and with electrical conductivity measurements of the noncalcined 25Nb@AlF_3 catalyst/water slurry, which indicated an increase of the electrical conductivity in water after 30 min at room temperature to 61 μS/cm (see Figure S5 in the Supporting Information). This clearly indicates the appearance of electrically charged ions, resulting from surface hydroxyl groups, during the contact of the noncalcined 25Nb@AlF_3 with water. On the other hand, the electrical conductivity of the 25Nb@AlF_3-500/water slurry remained unchanged, indicating a high stabilization of the solid structure during the calcination process.

A confirmation of the F/O exchange during the calcination process and of the surface "cleaning" during the water boiling is provided by a comparative investigation of the F(1s) (Figure 4), O(1s) (Figure 5), and Al(2p) (Figure 3) levels. The changes in the BE of the F(1s) and O(1s) levels are in line with the changes in the BE of the Al(2p) level. Except for the water-boiled 25Nb@AlF_3 sample, the binding energy of the F(1s) level in all samples was lower than that typical for α-AlF_3 (e.g., 686 eV), thus indicating a different chemical environment of F^- ions (Figure 4).[53] The F(1s) binding energy (681.9 eV) clearly reflects the presence of the residual electropositive −O*i*R coordinating groups. Increased temperatures led to an additional shift of the F(1s) BE (680 eV), most probably due to a further exchange of fluoride ions by oxygen (Figure 4). The strong decrease of the F(1s) band intensity at the same time as the increase in the O(1s) band intensity (Figures 4 and 5) supports this supposition as well.

XPS spectra in the region of the O(1s) level (Figure 5) show relatively broad and less intense peaks that, according to their deconvolution, reflect the presence of different oxygen species from the alkoxide and hydroxyl groups (Table S2 in the Supporting Information), at least for water-boiled or non-calcined samples.[54,55] Binding energies higher than 534 eV typically correspond to such OH groups.[56] After the samples were calcined at 350 and 500 °C, respectively, the peaks become narrower (some deconvolution components being completely vanished), indicating an increase in the oxygen

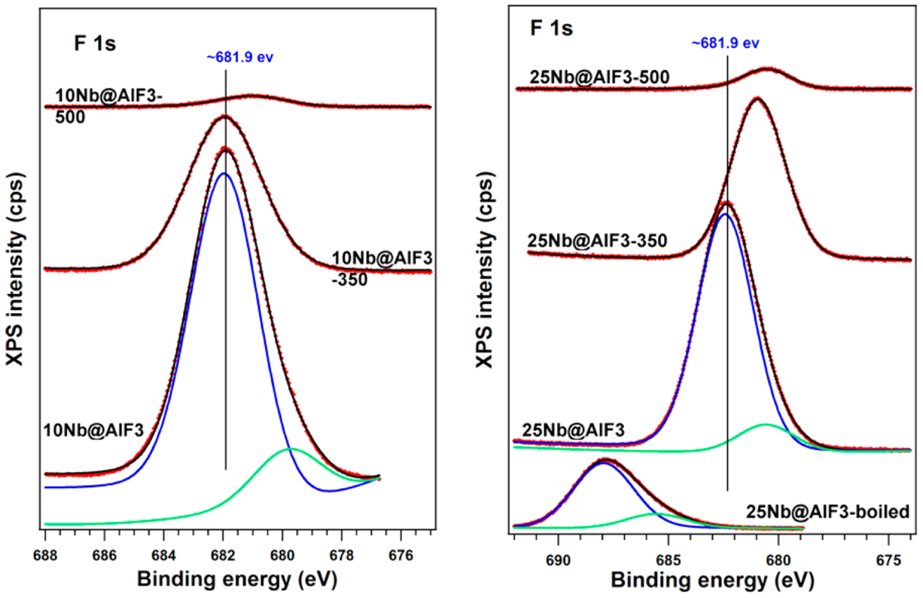

Figure 4. XPS spectra of the F(1s) level for the 10Nb@AlF_3 and 25Nb@AlF_3 samples.

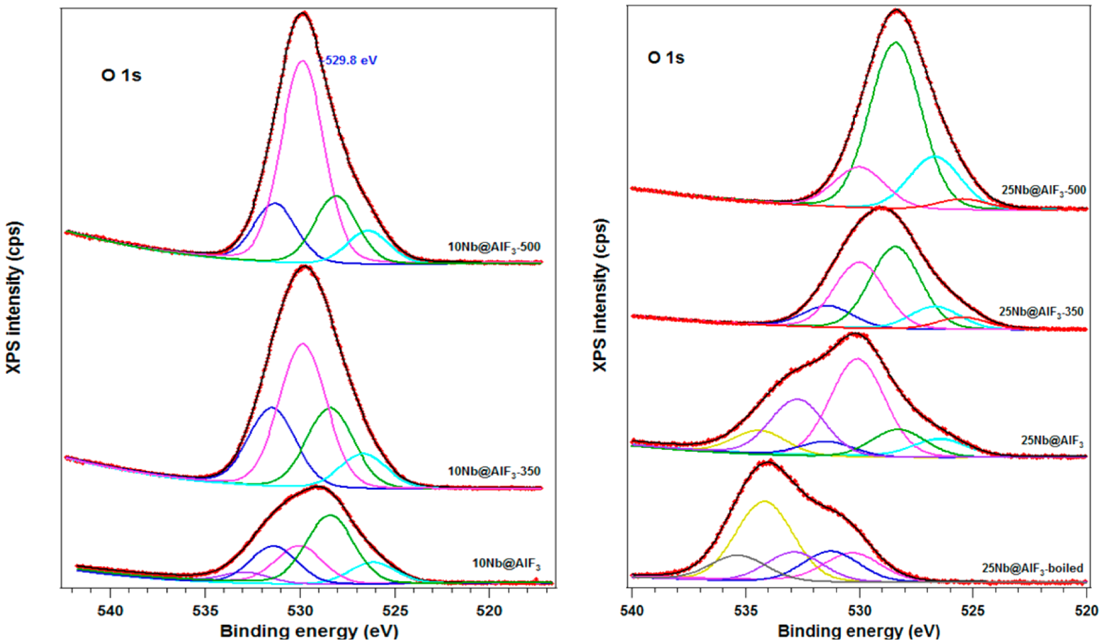

Figure 5. XPS spectra for the O(1s) level for the 10Nb@AlF$_3$ and 25Nb@AlF$_3$ samples.

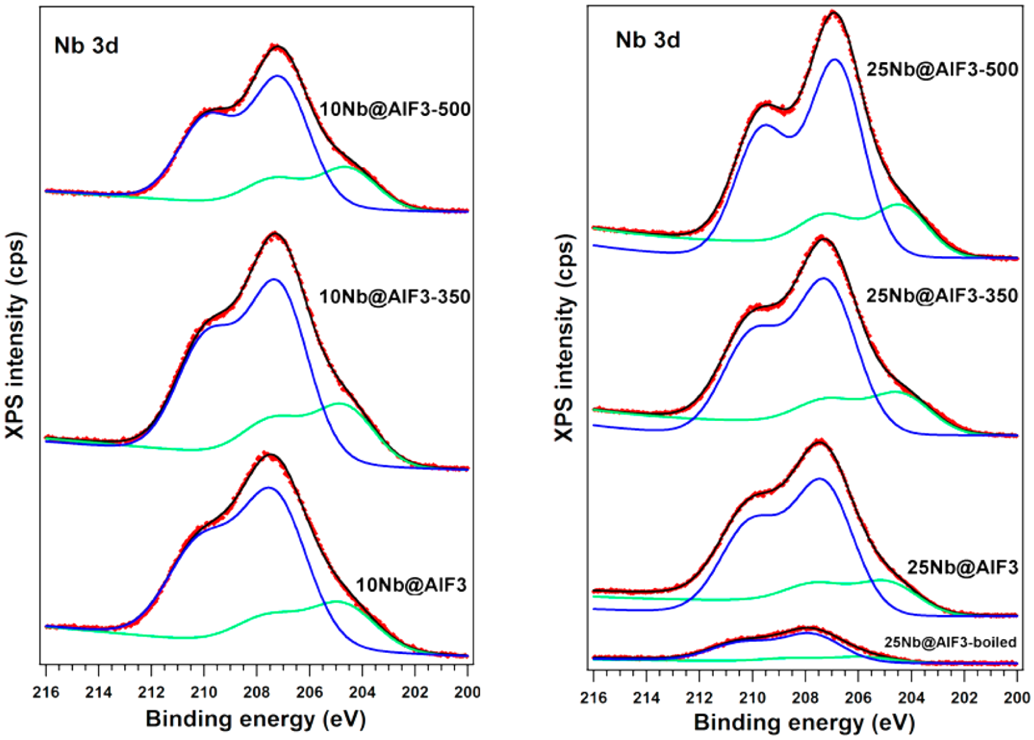

Figure 6. XP spectra for the Nb(3d) level for the 10Nb@AlF$_3$ and 25Nb@AlF$_3$ samples.

coordination, most probably due to the removal of OH and fluorine from the different AlF$_x$O$_{6-x}$ units and the formation of metal oxides, in agreement with NMR measurements.

XPS spectra of the Nb(3d) level for all samples are illustrated in Figure 6. Most of the Nb exists in the Nb^{5+} oxidation state (207.3 eV). However, a second component characterized by a lower BE located at 204.6 eV is present in all of these spectra, and it resulted from the synthesis. Most probably it might be assigned to Nb^{4+} species generated by the oxygen vacancies (loss of oxygen) produced during the synthesis.[57,58] This assignment correlates well with the NMR results, in which a Nb^{3+} species was not identified. The calcinations at 350 and 500 °C, respectively, do not affect this species as seen from the evolution of its intensity with temperature. However, the increase of the niobium content corresponded to a higher ratio between Nb^{4+} and Nb^{5+} species and is additionally caused by a partial loss of AlF$_3$, as discussed above. These spectra did not allow distinguishing between niobium coordinated by fluorine or oxygen.

Table 2 compiles the comparative chemical and XPS analysis results of the investigated catalysts. In comparison to the bulk composition, the XPS data indicate (i) a slightly higher

Table 2. Chemical Composition and Atomic XPS Concentration of Niobium-Doped Aluminum Hydroxyl Fluorides[a]

catalyst	chemical composition	atomic XPS concentration (%) Nb	Al	F	O	XPS ratio Nb/Al	Nb/F
$10Nb@AlF_3$	$AlNb_{0.09}F_{2.45}O_{0.63}$	6.61	26.22	44.78	22.39	0.25	0.15
$10Nb@AlF_3$-350	$AlNb_{0.11}F_{1.73}O_{0.92}$	6.29	28.92	22.29	42.50	0.22	0.28
$10Nb@AlF_3$-500	$AlNb_{0.11}F_{1.07}O_{1.27}$	5.66	33.51	2.10	58.73	0.17	2.70
$25Nb@AlF_3$	$AlNb_{0.23}F_{2.27}O_{0.54}$	8.41	21.98	48.14	21.47	0.38	0.17
$25Nb@AlF_3$-350	$AlNb_{0.23}F_{1.59}O_{0.91}$	7.08	27.92	21.39	43.61	0.25	0.33
$25Nb@AlF_3$-500	$AlNb_{0.24}F_{0.98}O_{1.24}$	6.65	31.8	2.71	58.84	0.21	2.45
$25Nb@AlF_3$-boiled	$AlNb_{0.33}F_{1.11}O_{1.12}$	5.38	27.6	42.06	24.95	0.19	0.13

[a] Al and Nb contents were determined by ICP-OES, and the F content was determined by the Seel method.[35]

concentration of niobium on the surface of the noncalcined materials, which is (ii) followed by a homogenization of niobium and aluminum after calcination. Both analyses confirmed the removal of fluorine during calcination. However, as XPS showed, it is merely extracted from the surface. As shown before, boiling of the noncalcined catalysts is merely extracting AlF_3.

Whereas Nb(V) is a nonmagnetic ion ($3d^04s^0$), Nb(IV) is a magnetic ($3d^14s^0$) ion with a spin $S = 1/2$, in specific anion surroundings leading to a high-spin configuration. On the other hand, AlF_xO_{6-x} configurations with the potential of changing the F/O ratio could constitute interesting diluted magnetic oxide/semiconductor (DMO/DMS) systems. It is worth mentioning that the recent interest in systems of transition-metal-substituted oxides originates from their room-temperature magnetism and potential applications in spintronic, magnetoelectronic, and optical devices.[59−61] In spite of considerable efforts to explain the presence of room-temperature magnetism in such systems, its origin is still under debate,[62,63] with one of the proposed mechanisms related to interacting magnetic entities through defects and or/oxygen vacancies. When all these aspects are taken into account, magnetic measurements might offer complementary information on defects/oxygen vacancies in the reported systems and, reciprocally, these specific systems might constitute interesting physical supports for elucidating the nature of their possible room-temperature magnetism.

Magnetic hysteresis loops at 300 K for noncalcined $25Nb@AlF_3$ and $25Nb@AlF_3$-boiled samples are shown in Figures 7 and 8, respectively.

In the case of the noncalcined $25Nb@AlF_3$ sample the coercive field at room temperature is of just 20(5) Oe, in spite of a more significant coercive field at 10 K of 160 Oe. On the other hand, a higher coercive field of 35(5) Oe was observed at room temperature in the $25Nb@AlF_3$-boiled sample in spite of just 40(5) Oe observed at 10 K. The presence of the hysteresis loop is a clear indication of a ferromagnetic phase, which when the linear increase of the magnetization versus field (at higher fields, as observed at room temperature) is taken into account has to be superposed over a paramagnetic component that is much more easily saturated at low temperatures.

The saturation magnetization at 10 K (reached above 5000 Oe for both samples) is about 7 times higher in the boiled sample, under conditions of almost similar relative contents of Nb(IV) ions in the two samples. Therefore, we may assume that the observed magnetism is not preponderantly related to the Nb(IV) species. While the observed magnetic behavior is similar to that observed in other DMO systems (superposed ferromagnetic and paramagnetic phases with the order temperature of the ferromagnetic phase higher than room temperature and coercive fields of tenths of Oe at room temperature), a mechanism related to defects (oxygen vacancies) will be tentatively assumed for its explanation. The magnetic order temperature (related to the exchange interaction strength) of the ferromagnetic phase is definitely much higher in the boiled sample, where the very slight decrease of the coercive field versus temperature is also supported by the almost constant dependence of the magnetization versus temperature (upper inset of Figure 8). By consideration of the ratio of Al positions in AlF_3 and

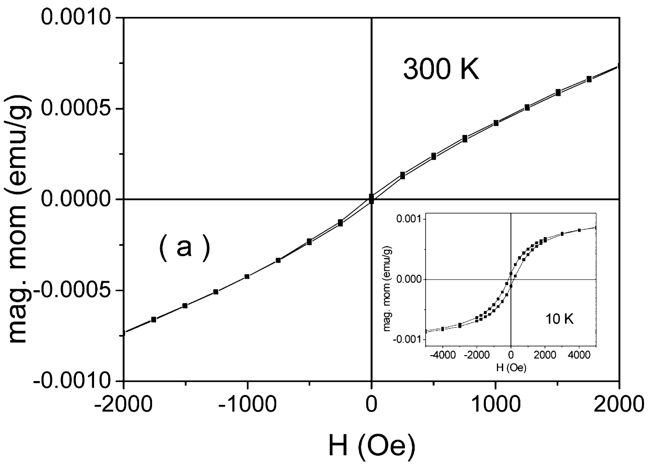

Figure 7. Hysteresis loop for $25Nb@AlF_3$ sample at 300 K. The inset shows the hysteresis loop collected at 10 K.

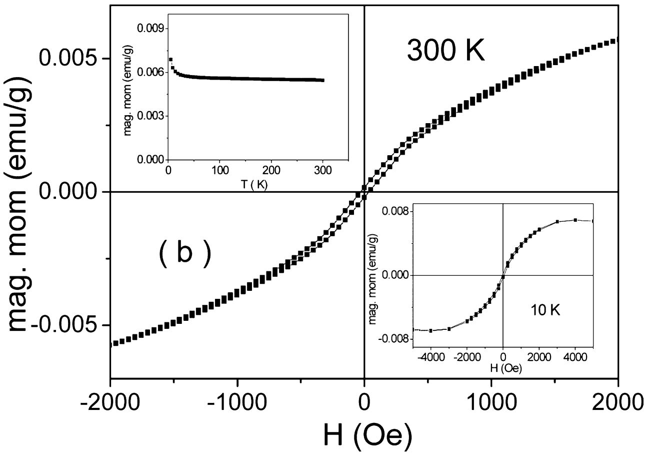

Figure 8. Hysteresis loop for $25Nb@AlF_3$-boiled sample, at 300 K. In the upper inset is shown the thermomagnetization curve obtained under a field of 2000 Oe whereas in the lower inset is shown the hysteresis loop collected at 10 K.

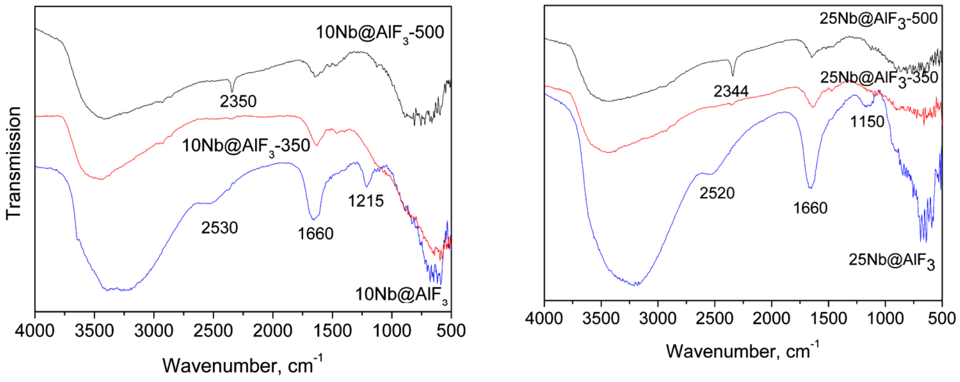

Figure 9. DRIFT spectra of the 10Nb@AlF$_3$ and 25Nb@AlF$_3$ samples.

AlF$_x$O$_{6-x}$ configurations provided by XPS, it is obvious that the number of AlF$_x$O$_{5-x}$ and AlF$_x$O$_{4-x}$ configurations is higher in the boiled sample, which might also explain the higher magnetization of this sample. At the same time, the XPS analysis shows shifted BE of Al (76.9 eV) in such positions, inferring enhanced oxygen vacancies at the AlF$_x$O$_{5-x}$ and AlF$_x$O$_{4-x}$ configurations of the boiled sample. Hence, the magnetic results give additional support to the XPS and ^{27}Al MAS NMR results and the aforementioned correlations sustain a mechanism with magnetic carriers depending on the number of oxygen-containing configurations (e.g., 6-fold coordinated Al units AlF$_x$O$_{6-x}$, 5-fold coordinated units AlF$_x$O$_{5-x}$, and 4-fold coordinated species AlF$_x$O$_{4-x}$) and the exchange interaction strength depending on the number of oxygen vacancies in such configurations.

DRIFT spectra were collected with the scope of further investigation of the framework presence of functional groups (Figure 9). The spectra of noncalcined samples present the typical vibrations of the surface OH groups and adsorbed H$_2$O at 1660 and 3000−3400 cm^{-1}. In addition, vibrations corresponding to CH$_3$ and CH at 2520 cm^{-1} (ν_{C-H}) and to the CO group (950−1300 cm^{-1}) characteristic for the alkoxides are present.

When the samples are purged with a nitrogen flow in order to ensure the evacuation of desorbed species, the isolated −OH group are better evidenced in the 3000−3400 cm^{-1} region (Figure 10). The right parts of the spectra are indicative of the metal−oxygen and metal−fluorine valence vibrations from 500 to 700 cm^{-1}, respectively, followed by the C−C frame absorptions of the organic constituents. The spectra of the amorphous products (noncalcined samples), i.e., 10Nb@AlF$_3$ and 25Nb@AlF$_3$, showed a strong but very broad band around 667 cm^{-1}, which is assigned to the Al−F stretch of corner-sharing AlF$_6$ octahedra. The width of this band and the absence of additional bands at 600 or 544 cm^{-1} are typical for highly amorphous aluminum fluoride compounds.[64]

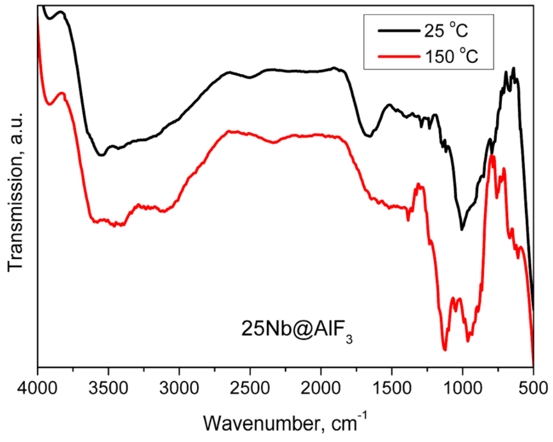

Figure 10. DRIFT spectra of the 25Nb@AlF$_3$ samples purged with a nitrogen flow.

In the case of calcined samples the position of this band is slightly shifted to 770 cm^{-1}, probably due to the different connectivities of the NbO$_x$F$_y$-AlF$_x$O$_{6-x}$ units and different lattice structures (i.e., AlF$_x$O$_{5-x}$ and AlF$_x$O$_{4-x}$ phases). Nevertheless, in all cases the absorption bands are broad, this phenomenon being directly related to the large degree of structural disorder present in these materials. Indeed, Raman spectroscopy (see Figure S6 in the Supporting Information) did not detect any niobium species in the noncalcined 10Nb@AlF$_3$ and 25Nb@AlF$_3$ samples that may correspond to a high degree of dispersion and the low crystallinity of the niobium species, which is in line with BET, XRD, and DRIFT results. On the other hand, for the calcined samples, the Raman spectra indicated a band located at 880 cm^{-1} that increased with the temperature and corresponded to niobyl groups (Nb═O) (see Figure S6), which is in accordance with the results of Montes and co-workers.[65]

The IR spectra (from 1400 to 1700 cm^{-1}) of pyridine (Py) adsorbed at 150 °C on 10Nb@AlF$_3$ and 25Nb@AlF$_3$ catalytic samples are shown in Figure 11. The specific IR absorption band centered at 1450 cm^{-1} can be related to Py coordinated to a Lewis site (LPy),while the specific IR wavelength from 1545 cm^{-1} is related to Py bonded to a Brønsted site (BPy), as previously reported.[66]

As Figure 11 shows, both dried (noncalcined) 10Nb@AlF$_3$ and 25Nb@AlF$_3$ samples displayed Lewis acid sites (associated with the noncoordinated Nb and Al sites) and Brønsted acid sites (which result from the −OH groups introduced during the preparation of the samples). While in the case of the 10Nb@AlF$_3$ sample Brønsted acid sites are still present even after calcination at 350 °C, in the case of 25Nb@AlF$_3$ the band at 1545 cm^{-1} almost vanished and only bands characteristic of strong Py adsorbed on Lewis acid sites between 1620 and 1600 cm^{-1} (gives information about the strength of Lewis acid sites) and between 1450 and 1440 cm^{-1} (related to the number of Lewis acid sites) were observed.

Interestingly enough, in the case of the 10Nb@AlF$_3$ sample calcined at 500 °C, the absorption maxima corresponding to Brønsted acid sites undergo a slight shift toward lower

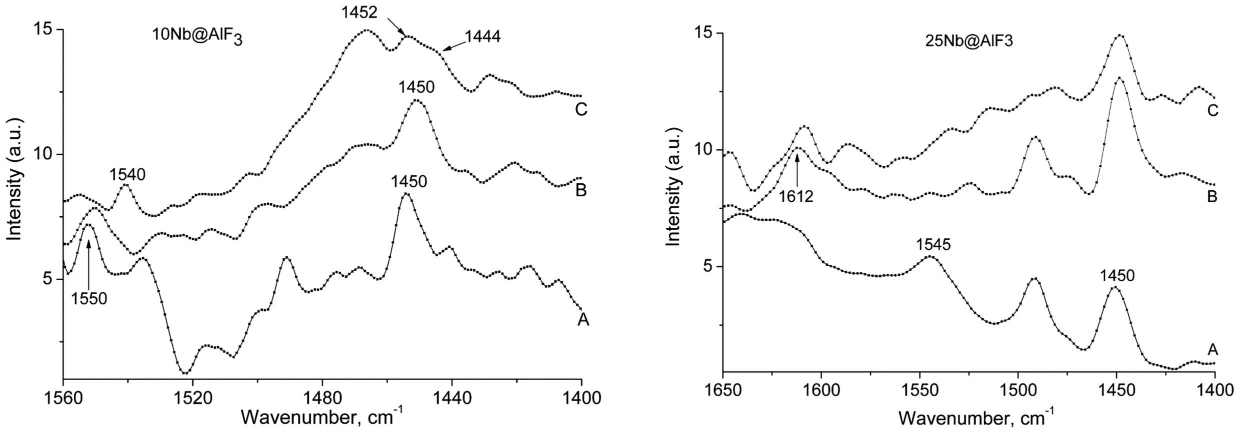

Figure 11. Py-IR spectra of the 10Nb@AlF$_3$ and 25Nb@AlF$_3$ samples: (A) noncalcined; (B) calcined at 350 °C; (C) calcined at 500 °C.

Table 3. Concentration and Density of the Lewis and Brønsted Acid Sites for Nb@AlF$_3$ Samples

			adsorption at 1450 cm^{-1} (PyL)		adsorption at 1540 cm^{-1} (PyB)	
catalyst	BET (m^2/g)	total acidity (μmol/g)	concn (μmol/g)	density (molecules/nm^2)	concn (μmol/g)	density (molecules/nm^2)
10Nb@AlF$_3$	251	32.1	20.5	0.05	11.6	0.03
10Nb@AlF$_3$-350	203	53.9	35.9	0.11	18.0	0.05
10Nb@AlF$_3$-500	69	16.7	10.3	0.10	6.4	0.05
25Nb@AlF$_3$	213	82.7	58.2	0.16	24.5	0.07
25Nb@AlF$_3$-350	137	59.5	58.2	0.26	1.3	0.01
25Nb@AlF$_3$-500	63	25.7	25.7	0.24	0	0

Scheme 1. Schematic Representation of the Lewis/Brønsted Acid Sites in Catalytic Materials

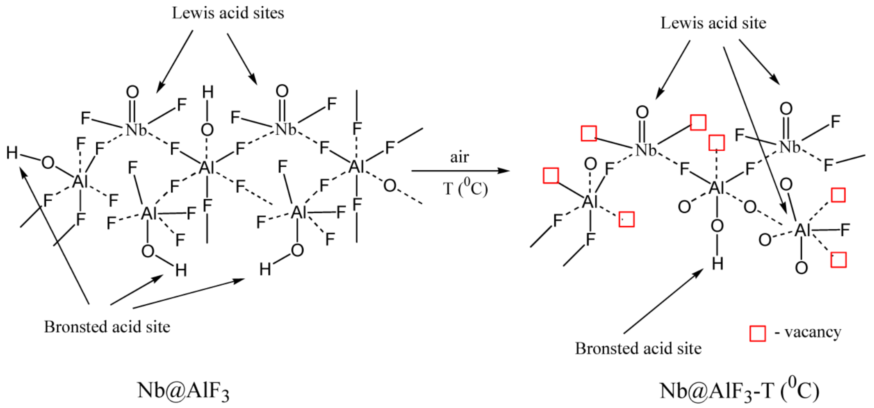

frequencies (from 1550 to 1540 cm^{-1}, spectra C in Figure 11) while the band characteristic of Lewis acid sites (1450 cm^{-1}) is weakened and splits into two absorption maxima at 1444 and 1452 cm^{-1}. These shifts could be attributed to a solvation effect of the solid framework, similar to that observed for zeolites.[67] This effect toward the adsorbed species is similar to that of an aprotic dipolar solvent.

This hypothesis was confirmed by Glazumov and Odinokov[68] by dissolving Py in a mixture with a dipolar aprotic solvent, where a pyridinium ion showing a maximum absorption at 1537 cm^{-1} was evidenced. The 25Nb@AlF$_3$-500 sample displayed a similar IR spectrum with the 25Nb@AlF$_3$-350 sample, but the bands were slightly attenuated. Preponderantly strong Lewis acid sites were evidenced, while Brønsted sites were visible only as traces. Indeed, the fluorides and oxide fluorides of early transition metals in high oxidation states are strong Lewis acids and form a substantial range of compounds with F$^-$ and O^{2-}.[35]

In the case of Nb$_2$O$_5$/MO$_x$ catalysts, Maurer and Ko[69] showed that Nb═O bonds, associated with Lewis acid sites, belong to highly distorted NbO$_6$ octahedra. Due to the removal of coordinated water, the dehydration process further distorts the already highly distorted NbO$_6$ octahedra, increasing the strength of Lewis acid sites. In contrast, the slightly distorted NbO$_6$ octahedra as well as the NbO$_7$ and NbO$_8$ groups possess only Nb−O bonds and are associated with Brønsted acid sites (e.g., in Nb$_2$O$_5$/Al$_2$O$_3$ and Nb$_2$O$_5$/SiO$_2$ systems). Lewis acid sites are present in all supported niobium oxide systems.[70,71] In correlation with these data and taking into account the results obtained from Py-IR (Figure 11) and Raman spectra (Figure S6 in the Supporting Information), the existence of different NbO$_x$F$_y$ phases interconnected with AlO$_x$F$_y$ phases, in different proportions, as a function of the content in niobium and calcination temperature can be easily concluded. CO$_2$-TPD measurements showed no basicity for the investigated catalysts.

Table 4. Catalytic Performance as a Function of the Calcination Temperature[a]

entry	catalyst	Brønsted AS (μmol/g)	X (%)	Lewis AS (μmol/g)	L/B ratio	Y_i (%) LA	GA	2-HBA	Y_{liquid} (%)	E_c
1	10Nb@AlF$_3$	11.6	39	20.5	1.8	4.7	2.6	2.4	9.7	24.8
2	10Nb@AlF$_3$-350	18.0	31	35.9	2.0	14.3	3.9	2.0	20.2	65.1
3	10Nb@AlF$_3$-500	6.4	24	10.3	1.6	7.0	1.8	1.3	10.1	42.1
4	25Nb@AlF$_3$	24.5	35	58.2	2.4	6.9	3.8	2.8	13.5	38.6
5	25Nb@AlF$_3$-350	1.3	29	58.2	44.8	20.0	3.5	2.5	26.0	89.5
6	25Nb@AlF$_3$-500	0	20	25.7		2.8	1.3	0.6	4.7	23.3

[a]Reaction conditions: 180 °C, 30 mL of water, 0.56 g of cellulose, 0.056 g of catalyst, 1000 rpm, 24 h. Abbreviations: LA, lactic acid; GA, glycolic acid; 2HBA, 2-hydroxybutanoic acid.

Scheme 2. Two-Step Homogeneous/Heterogeneous Mechanism of the Hydrolysis of Cellulose to Glucose

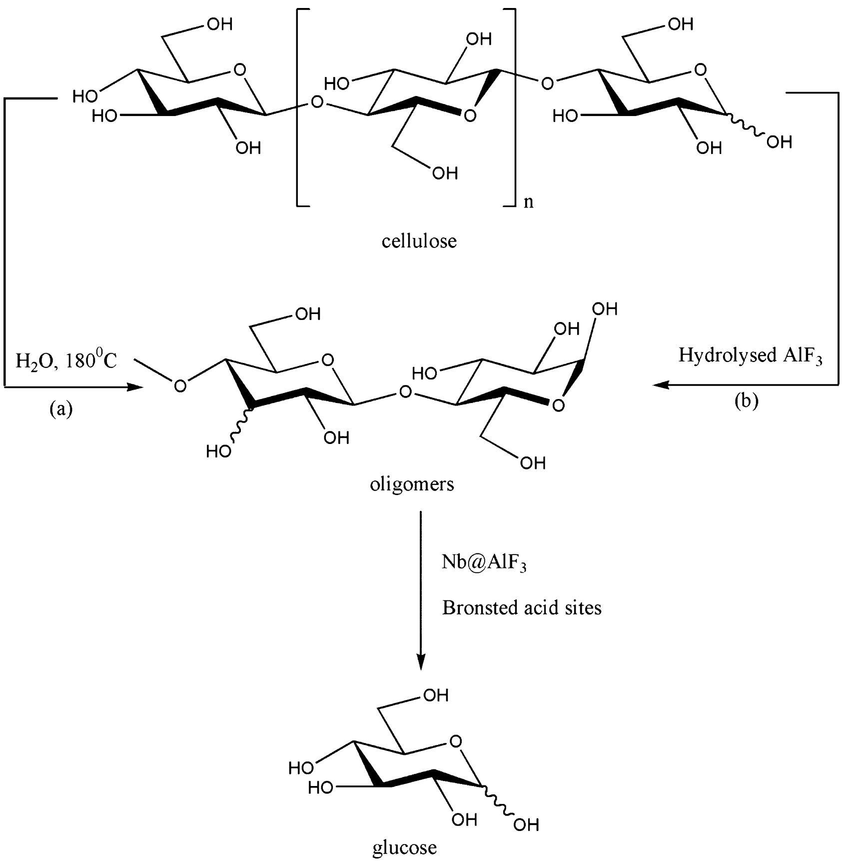

The surface Brønsted and Lewis acid site distribution was determined from the same Py-FTIR measurements, taking into consideration the integrated Lambert−Beer law.[67] For the estimation of Brønsted and Lewis acid site populations, Corma[72] recommends the general use of published extinction coefficients (ε_I), typically obtained by one of the following transmission IR-coupled methods: selective elimination of Brønsted acidity followed by water vapor exposure,[73] dosing of known amounts of pyridine,[74] or water vapor exposure to convert Lewis acidity into Brønsted acidity.[75]

Using this approach the most suitable bands for a quantitative evaluation are those at 1450 and 1550 cm^{-1}, corresponding to Lewis and Brønsted sites, respectively. Among the ε_I values available in the literature,[74,76−79] those calculated by Emeis[77] ($\varepsilon_{I,B}$ = 1.67 ± 0.12 cm/μmol; $\varepsilon_{I,L}$ =2.22 ± 0.21 cm/μmol) seem to be the most reliable for our purposes. Accordingly, the concentration of Brønsted and Lewis acid sites referenced to the weight of the sample (q_H (μmol/g)) has been obtained according to

$$q_H = \frac{A_I \pi R^2}{w \varepsilon_I} \tag{4}$$

where A_I is the integrated absorbance, R (cm) is the radius of the catalyst wafer, ε_I is the extinction coefficient, and w (g) is the weight of the sample.[67]

These parameters are compiled in Table 3. Scheme 1 gives a schematic representation of the Lewis/Brønsted acid sites in these materials.

Within group V, the oxide fluorides, MOF$_3$, are intractable and have been studied very little.[80] However, on the surface of the catalysts during the calcination on the basis of the characterization results, the formation of different oxide fluoride species, along with 6-fold coordinated Al units AlF$_x$O$_{6-x}$, 5-fold coordinated units AlF$_x$O$_{5-x}$, and 4-fold coordinated species

Table 5. Catalytic Results using Preboiled 25Nb@AlF_3 and Leached Aluminum Hydroxydefluoride[a]

					yield (%)				
entry	catalyst	Brønsted AS (μmol/g)	X (%)	Lewis AS (μmol/g)	LA	GA	2-HBA	Y_{liquid} (%)	E_c
1	fresh 25Nb@AlF_3	24.5	43	58.2	17.0	4.9	5.1	27.0	62.8
2	preboiled 25Nb@AlF_3	1.7	34	24.8	27.3	6.7	0	34.0	100
3	separated liquid phase with leached AlF_3		74		5.9	4.7	0	10.6	14.4
4	AlF_3-50		70		2.1	3.2	0	5.3	7.8

[a] Reaction conditions: 180 °C, 5 mL of water, 0.16 g of cellulose, 0.06 g of catalyst, reaction time 2 h, 1000 rpm.

AlF_xO_{4-x}, cannot be excluded. The niobium (Nb(V) and Nb(IV)) species are distributed in both crystalline and amorphous phases. Nb(V) exists in different environments with low crystallinity (see XRD in the Supporting Information) while Nb(IV) is merely distributed in the amorphous part of the solid in close association with the evidenced oxygen vacancies (XPS, NMR, and magnetic measurements).

The calcination of the catalytic samples influences the catalytic performances in terms of conversion, yields toward the reaction products, and carbon efficiency (E_c) (Table 4). E_c expresses the overall selectivity to the desired liquid-phase products. It was calculated from the ratio of the weight of hydroxy acids in the product mixture to the weight of cellulose transformed during the reaction. The term "desired" may be defined differently depending on the aim of the study. Herein, we considered the products dissolved in the water phase as desirable, while gaseous compounds (such as methane or carbon dioxide) and water-soluble oligomers/humins, which cannot be analyzed by GC-FID/GC-MS, as undesired.

As Table 4 shows, higher conversions of cellulose can be reached on noncalcined catalysts, irrespective of the niobium content. It decreases with the increase of the calcination temperature that corresponds in fact to a less defected catalyst structure. For the high temperature calcined catalysts, under the harsh reaction conditions, the only species able to initiate hydrolyzing of cellulose to smaller oligomers are acidified water molecules. Such a supposition is also supported by a conversion level of 20% (Table 4, entry 6) obtained in the presence of the 25Nb@AlF_3-500 sample. No leaching of aluminum (only 25 ppm) was determined for this catalyst (ICP-OES measurements, Supporting Information).

The ICP-OES measurement after each reaction showed an insignificant leaching of Nb species in a range of 1−3 ppm, while aluminum fluoride leached in higher but different amounts, as a function of the calcination pretreatments. Thus, around 200 ppm of aluminum was leached from the dried catalysts to the aqueous phase during the catalytic reaction, irrespective of the niobium content (e.g., 10 or 25%). The calcination of the samples somehow stabilized the solid structure by complete reorganization of the structure through the formation of oxide fluoride phases, and the leaching of aluminum was diminished from 70 to 15 ppm, after the increase of the calcination temperature from 350 to 500 °C. These results are not surprising, since it is well-known that aluminum fluoride is soluble in water (1.72 g/100 mL at 100 °C), forming hydrated aluminum fluoride species.[81] Taking into account the ICP-OES and electric conductivity measurements, it is clear that while part of the AlF_3 species are leached in the reaction medium as hydrolyzed aluminum fluoride, the solid material became enriched in Nb species.

In the presence of noncalcined Nb@AlF_3 samples the higher conversions (Table 4, entries 1 and 4) are assigned to AlF_3 species released by the solid material, also catalyzing the partial hydrolysis of cellulose to oligomers (e.g., cellobiose, cellotriose, etc.) and glucose. It can be therefore speculated that the hydrolysis of cellulose takes place following a two-step homogeneous/heterogeneous mechanism in which an initial partial hydrolysis proceeds in the presence of leached AlF_3 species as hydrolyzed aluminum fluorides and/or under the effect of water at the high temperature (Scheme 2). The heterogeneous catalytic process starts only in the moment when the hydrolysis generates oligomers small enough to penetrate the catalyst pore system, leading to the reaction products.

In accordance with the literature, the synthesis of lactic acid from hexoses is greatly influenced by the acidity of the solid catalysts.[82−85] Indeed, examining the results obtained in this study, 25Nb@AlF_3-350 seems to display an optimum L/B ratio (Table 4, entry 5) for the water-soluble glucose isomerization/esterification to lactic acid. In contrast to zeolite materials used as catalysts in the synthesis of methyl lactate from trioses or hexoses,[86] niobium-based catalysts display a remarkably high acidity and a high hydrothermal stability,[19,27−29] inducing a great advantage for the biomass transformations. When the calcination temperature was increased from 350 to 500 °C, the Brønsted acidity decreased in favor of the Lewis acidity. Unfortunately, this does not correspond to an increase of the yield in lactic acid, as expected. Obviously, due to the polar and protic properties of water, some of the Lewis sites may interact with this molecule during the reaction in aqueous media. In this case, as was recently reported by Carniti et al.[87,88] for niobic acid, niobium phosphate, and silica-niobium oxide systems, the number, strength, and nature of acid sites from the surface of the catalyst will not follow the typical trend determined by Py-IR techniques. Thus, taking into account the obtained catalytic results, and in accordance with the above studies, the catalyst acidity in the water phase can be directly associated with the presence of niobium acid sites.

As the ICP-OES and surface area measurements showed, calcination corresponds not only to structural changes leading to a hydro-stabilization of the catalyst but also to a decrease in the surface area, accompanied by crystallization and some collapses (see XRD analysis, in the Supporting Information). These changes induce mass transfer limitations that are responsible, at least partially, for the decrease of the yield in reaction products.

As specified above, in the presence of the noncalcined samples (e.g., 10Nb@AlF_3 and 25Nb@AlF_3), both the yield in lactic acid and E_c greatly decreased in comparison with those for the calcined samples. These catalysts are not stable under the reaction conditions, and ICP-OES measurements showed a high amount of leached aluminum fluoride. Therefore, a question that arose was as follows: to what extent may the leached aluminum hydroxide fluoride species influence the reaction performances? To answer this question, some additional cellulose degradation tests were done in which boiled 25Nb@AlF_3 in pure water at 180 °C for 2 h was used as catalyst. Moreover, the separated solution from this pretreatment, which contained leached aluminum hydroxide fluoride (915 ppm Al^{3+}), was used as a "homogeneous catalyst" in a separate experiment. The results are given in Table 5.

As Table 5 shows, the 25Nb@AlF_3 sample recovered after the separation of leached aluminum species became highly selective to hydroxy acids, with a preponderant formation of lactic acid, while the conversion of cellulose decreased ny only few percen in comparison with the fresh catalyst (Table 5, entry 1).

In line with magnetic, XPS, NMR, and ICP-OES measurements, the leaching of aluminum enriched the catalyst in niobium oxide fluoride phases (the boiled catalyst contains 42.5 mol % of Nb and 57.5 mol % of Al in comparison to fresh catalyst, which contains 25 mol % of Nb and 75 mol % of Al) alongside the introduction of an oxygen/aluminum vacancy adjacent to the niobium sites ($NbOF_x$, Lewis acid sites), by the formation of different 6-fold coordinated Al units AlF_xO_{6-x}, 5-fold coordinated units AlF_xO_{5-x}, and 4-fold coordinated species AlF_xO_{4-x}, thus creating an optimum combination of acidity for the one-pot transformation of cellulose to lactic acid.

Experiments with the separated liquid phase showed that in accordance with its acidity (pH 2.05) it is able to catalyze the depolymerization of cellulose to a great extent (74.0% in 2 h), but only with the formation of insignificant amounts of lactic acid. As was mentioned above, the acidity is ensured by the presence of aluminum hydroxide fluoride species exhibiting a Brønsted acid character and HF generated during the hydrolysis. Similar results were obtained in the presence of free niobium AlF_3-50 sample (Table 5, entry 4), where a high conversion to cellulose was measured with almost no yield of lactic acid. These results complete the results obtained on calcined catalysts, indicating that, indeed, the active sites responsible for the lactic acid formation are the niobium species incorporated in amorphous/crystalline phases of the catalysts. Thus, the yield in lactic acid increases from 14.3% to 20.0% for 10Nb@AlF_3-350 and 25Nb@AlF_3-350, respectively, and from 17.0% to 27.3% for 25Nb@AlF_3 and boiled 25Nb@AlF_3 (with 42.5% Nb after boiling according to ICP-OES analysis).

In addition to the loading, the oxidation state of niobium has also a significant effect on the yield of lactic acid. Figure 12 indeed shows a good correlation between the Nb^{4+}/Nb^{5+} ratio determined from XPS measurements and the yield in lactic acid. The increase of this ratio produces smaller yields in lactic acid. Such a variation can be explained when considering the presence of Nb(IV) in close association with the oxygen vacancies. During the catalytic process, these vacancies can be occupied by the water molecules blocking the access of the glucose molecules.

For the production of lactic acid a mechanism is commonly claimed which involves glucose isomerization to fructose and retro-aldol condensation of fructose followed by triose isomerization to lactic acid, all of these reaction sentences being catalyzed by Lewis acid sites[17] (see Scheme S2 in the Supporting Information).

The data obtained indicate that, although Brønsted acidity favors the hydrolysis of olygomers, an excess of these species does not help a further transformation of glucose to lactic acid but would be responsible for different side reactions such as (i) dehydration of the sugars to levulinic acid and methylpyranoside (see also the early reports of Rivalier et al.[84]), (ii) the cleavage of 1,3-dihydroxyacetone to glycolaldehyde and formaldehyde with the subsequent oxidation of the carbonyl group to glycolic acid (GA), and (iii) the aldolization/dehydration reaction between methylglyoxal and formaldehyde to ethylglyoxal followed by its hydration to 2-hydroxybutanoic acid (2-HBA) (Scheme S2 in the Supporting Information).

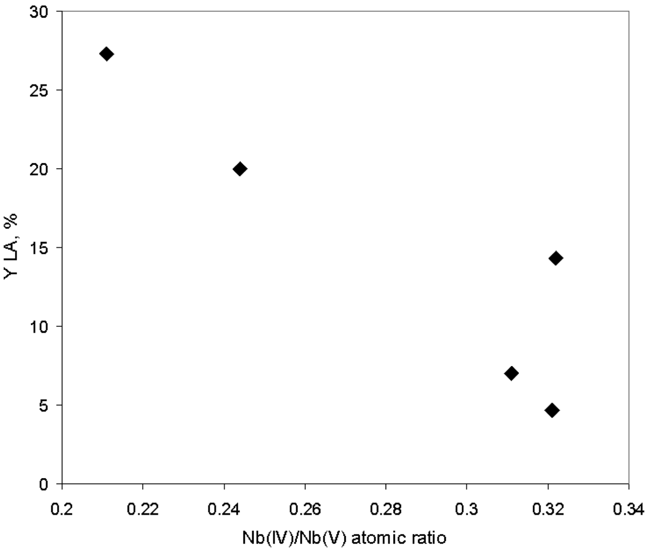

Figure 12. Relationship between Nb^{4+}/Nb^{5+} ratios and the yield in lactic acid.

A relatively low conversion of cellulose is not necessarily a disadvantage of the process. Low glucose working concentrations are important to avoid competitive side reactions such as condensation and dehydration to insoluble humins.[82]

To the best of our knowledge these results are superior to those reported in the literature for the one-pot synthesis of lactic acid from cellulose. Chambon et al.[89] showed, for instance, that solid Lewis acid catalysts such as tungstated zirconia and tungstated alumina exhibited a remarkable promoting effect on cellulose depolymerization, leading to a 27% lactic acid yield at 190 °C and 24 h, while Liu et al.[90] used a solid base MgO catalyst to achieve similar yields in methanol at 200 °C for 20 h.

4. CONCLUSIONS

A series of niobium-modified aluminum hydroxide fluorides prepared via the fluorolytic sol−gel synthesis by reacting aluminum/niobium alkoxides with anhydrous hydrogen fluoride in ethanol was investigated for the catalytic conversion of cellulose into lactic acid. FTIR pyridine adsorption investigations demonstrated that, by doping aluminum fluoride with niobium, the acidity of the resulted catalysts was significantly improved. Calcination of these catalysts stabilizes the structure and generated Lewis acidity that increased with the calcination temperature, while the Brønsted acidity decreased irrespective of the niobium loading.

Another route to create selective catalysts is the removal of aluminum from the solid network by preboiling of the solid, thus creating adjacent vacancies and/or free coordinations next to niobium sites.

The catalytic results confirm that the active sites responsible for the lactic acid formation from glucose (i.e., through reaction sequences involving the glucose isomerization to fructose and retro-aldol condensation of fructose followed by the triose isomerization) are the Nb(V)/Nb(IV) species from amorphous/crystalline phases, diluted in the aluminum oxide fluoride matrix.

In conclusion, the new niobium oxide fluoride based catalysts provide an optimum combination of active sites for the one-pot transformation of cellulose to lactic acid. The system presented here is still under investigation by our groups for further optimizations.

ASSOCIATED CONTENT

Supporting Information

The following file is available free of charge on the ACS Publications website at DOI: 10.1021/acscatal.5b00282.

> Catalyst characterization (XRD, adsorption−desorption isotherms of liquid nitrogen, Raman spectroscopy, conductivity measurements) and GC-MS analysis of the reaction products (PDF)

AUTHOR INFORMATION

Corresponding Authors

*S.M.C.: tel/fax, +40 21 410 02 41; e-mail, simona.coman@g.unibuc.ro.
*V.I.P.: e-mail, vasile.parvulescu@g.unibuc.ro.
*E.K.: e-mail, erhard.kemnitz@chemie.hu-berlin.de.

Notes

The authors declare no competing financial interest.

ACKNOWLEDGMENTS

The work was supported by the strategic grant POSDRU/89/1.5/S/58852, Project "Postdoctoral programme for training scientific researchers", cofinanced by the European Social Foundation within the Sectorial Operational Program Human Resources Development 2007−2013. S.M.C. kindly acknowledges the UEFISCDI for financial support (project PN-II-PCCA-2011-3.2-1367, Nr. 31/2012), whereas V.K. acknowledges financial support through the project PN-II-PCE 75/2011. The authors kindly acknowledge Dr. Florentina Neatu for part of the XPS measurements and Dr. Kerstin Scheurell for catalyst preparation.

REFERENCES

(1) Chew, T. L.; Bhatia, S. *Bioresour. Technol.* **2008**, *99*, 7911−7922.

(2) Van de Vyver, S.; Geboers, J.; Jacobs, P. A.; Sels, B. F. *ChemCatChem* **2011**, *3*, 82−94.

(3) Komanoya, T.; Kobayashi, H.; Hara, K.; Chun, W.-J.; Fukuoka, A. *Appl. Catal., A* **2011**, *407*, 188−194.

(4) Pereira, C. S. M.; Silva, V. M. T. M.; Rodrigues, A. E. *Green Chem.* **2011**, *13*, 2658−2671.

(5) Jang, T. Y.; Chung, K. B.; Eom, H. R.; Noh, D. K.; Song, I. K.; Yi, J.; Baeck, S.-H. *Res. Chem. Intermed.* **2011**, *37*, 1275−1282.

(6) Simonov, M. N.; Zaikin, P. A.; Simakova, I. L. *Appl. Catal., B* **2012**, *119−120*, 340−347.

(7) Takeda, Y.; Shoji, T.; Watanabe, H.; Tamura, M.; Nakagawa, Y.; Okumura, K.; Tomishige, K. *ChemSusChem* **2015**, *8*, 1170−1178.

(8) Castillo Martinez, F. A.; Balciunas, E. M.; Salgado, J. M.; Dominguez Gonzalez, J. M.; Converti, A.; Oliveira, R. P. D. S. *Trends Food Sci. Technol.* **2013**, *30*, 70−83.

(9) Zhang, J.; Zhao, Y.; Feng, X.; Pan, M.; Zhao, J.; Ji, W.; Au, C.-T. *Catal. Sci. Technol.* **2014**, *4*, 1376−1385.

(10) Yan, X.; Jin, F.; Tohji, K.; Moriya, T.; Enomoto, H. *J. Mater. Sci.* **2007**, *42*, 9995−9999.

(11) Ryabenkova, Y.; He, Q.; Miedziak, P. J.; Dummer, N. F.; Taylor, S. H.; Carley, A. F.; Morgan, D. J.; Dimitratos, N.; Willock, D. J.; Bethell, D.; Knight, D. W.; Chadwick, D.; Kiely, C. J.; Hutchings, G. J. *Catal. Today* **2013**, *203*, 139−145.

(12) Hayashi, Y.; Sasaki, Y. *Chem. Commun.* **2005**, *21*, 2716−2718.

(13) Janssen, K. P. F.; Paul, J. S.; Sels, B. F.; Jacobs, P. A. *Stud. Surf. Sci. Catal.* **2007**, *170*, 1222−1227.

(14) Taarning, E.; Saravanamurugan, S.; Holm, M. S.; Xiong, J.; West, R. M.; Christensen, C. H. *ChemSusChem* **2009**, *7*, 625−627.

(15) West, R. M.; Holm, M. S.; Saravanamurugan, S.; Xiong, J.; Beversdorf, Z.; Taarning, E.; Christensen, C. H. *J. Catal.* **2010**, *269*, 122−130.

(16) Li, L.; Stroobants, C.; Lin, K.; Jacobs, P. A.; Sels, B. F.; Pescarmona, P. P. *Green Chem.* **2011**, *13*, 1175−1181.

(17) Holm, M. S.; Saravanamurugan, S.; Taarning, E. *Science* **2010**, *328*, 602−605.

(18) Osmundsen, C. M.; Holm, M. S.; Dahl, S.; Taarning, E. *Proc. R. Soc. London, Ser. A* **2012**, *468*, 2000−2016.

(19) Pârvulescu, V.; Ruwet, M.; Grange, P.; Pârvulescu, V. I. *J. Mol. Catal. A: Chem.* **1998**, *135*, 75−88.

(20) Oliveira, L. C. A.; Ramalho, T. C.; Souza, E. F.; Gonçalves, M.; Oliveira, D. Q. L.; Pereira, M. C.; Fabris, J. D. *Appl. Catal., B* **2008**, *83*, 169−176.

(21) Silva, A. C.; Oliveira, D. Q. L.; Oliveira, L. C. A.; Anastácio, A. S.; Ramalho, T. C.; Lopes, J. H.; Carvalho, H. W. P.; Torres, C. E. R. *Appl. Catal., A* **2009**, *357*, 79−84.

(22) Guimaraes, I. R.; Oliveira, L. C. A.; Queiroz, P. F.; Ramalho, T. C.; Pereira, M. C.; Fabris, J. D.; Ardisson, J. D. *Appl. Catal., A* **2008**, *347*, 89−93.

(23) Nowak, I.; Ziolek, M. *Chem. Rev.* **1999**, *99*, 3603−3624.

(24) West, R. M.; Braden, D. J.; Dumesic, J. A. *J. Catal.* **2009**, *262*, 134−143.

(25) Pagán-Torres, Y. J.; Gallo, J. M. R.; Wang, D.; Pham, H. N.; Libera, J. A.; Marshall, C. L.; Elam, J. W.; Datye, A. K.; Dumesic, J. A. *ACS Catal.* **2011**, *1*, 1234−1245.

(26) Pham, H. N.; Pagan-Torres, Y. J.; Serrano-Ruiz, J. C.; Wang, D.; Dumesic, J. A.; Datye, A. K. *Appl. Catal., A* **2011**, *397*, 153−162.

(27) Ziolek, M. *Catal. Today* **2003**, *78*, 47−64.

(28) Shiju, N. R.; Brown, D. R.; Wilson, K.; Rothenberg, G. *Top. Catal.* **2010**, *53*, 1217−1223.

(29) Weissman, J. G. *Catal. Today* **1996**, *28*, 159−166.

(30) Tanabe, K. *Bull. Chem. Soc. Jpn.* **1974**, *47*, 1064−1066.

(31) Kemnitz, E.; Zhu, Y.; Adamczyk, B. *J. Fluorine Chem.* **2002**, *114*, 163−170.

(32) Wuttke, S.; Negoi, A.; Gheorghe, N.; Kuncser, V.; Kemnitz, E.; Parvulescu, V. I.; Coman, S. M. *ChemSusChem* **2012**, *5*, 1708−1711.

(33) Coman, S. M.; Wuttke, S.; Vimont, A.; Daturi, M.; Kemnitz, E. *Adv. Synth. Catal.* **2008**, *350*, 2517−2524.

(34) Teodorescu, C. M.; Esteva, J. M.; Karnatak, R. C.; El Afif, A. *Nucl. Instrum. Methods Phys. Res., Sect. A* **1994**, *345*, 141−147.

(35) Scheurell, K.; Kemnitz, E. *J. Mater. Chem.* **2005**, *15*, 4845−4853.

(36) Cory, D. G.; Ritchey, W. M. *J. Magn. Reson.* **1988**, *80*, 128−132.

(37) Kemnitz, E.; Hess, A.; Rother, G.; Troyanov, S. *J. Catal.* **1996**, *159*, 332−339.

(38) Xiang, Q.; Lee, Y. Y.; Pettersson, P. O.; Torget, R. W. *Appl. Biochem. Biotechnol.* **2003**, *105−108*, 505−514.

(39) Rinaldi, R.; Palkovits, R.; Schüth, F. *Angew. Chem., Int. Ed.* **2008**, *47*, 8047−8050.

(40) König, R.; Scholz, G.; Bertram, R.; Kemnitz, E. *J. Fluorine Chem.* **2008**, *129*, 598−606.

(41) König, R.; Scholz, G.; Pawlik, A.; Jäger, C.; van Rossum, B.; Oschkinat, H.; Kemnitz, E. *J. Phys. Chem. C* **2008**, *112*, 15708−15720.

(42) König, R.; Scholz, G.; Pawlik, A.; Jäger, C.; van Rossum, B.; Kemnitz, E. *J. Phys. Chem. C* **2009**, *113*, 15576−15585.

(43) Stosiek, C.; Scholz, G.; Eltanany, G.; Bertram, R.; Kemnitz, E. *Chem. Mater.* **2008**, *20*, 5687−5697.

(44) Kavun, V. Ya.; Gabuda, S. P.; Kozlovam, S. G.; Tkachenko, I. A.; Laptash, N. M. *J. Fluorine Chem.* **2011**, *132*, 698−702.

(45) Rakhmatullin, A.; Cibulkova, J.; Fayon, F.; Von Barner, J. H.; Bessada, C.; Massiot, D. 1st EENC/AMPERE joint meeting, Lille, France, 2004.

(46) McGuire, G. E.; Schweitzer, G. Kk.; Carlson, T. A. *Inorg. Chem.* **1973**, *12*, 2451−2453.

(47) Barr, T. L. *Appl. Surf. Sci.* **1983**, *15*, 1−35.

(48) Verziu, M.; Florea, M.; Simon, S.; Simon, V.; Filip, P.; Parvulescu, V. I.; Hardacre, C. *J. Catal.* **2009**, *263*, 56−66.

(49) Turner, N. H.; Single, A. M. *Surf. Interface Anal.* **1990**, *15*, 215−222.

(50) Gillet, E.; Ealet, B. *Surf. Sci.* **1992**, *273*, 427−437.

(51) Heß, A.; Kemnitz, E.; Lippitz, A.; Unger, W. E. S.; Menz, D.-H. *J. Catal.* **1994**, *148*, 270−280.

(52) Lindsay, J. R.; Rose, H. J.; Swartz, W. E.; Watts, P. H.; Rayburn, K. A. *Appl. Spectrosc.* **1973**, *27*, 1−5.

(53) Herron, N.; Thorn, D. L.; Harlow, R. L.; Jones, G. A.; Parise, J. B.; Fernandez-Baca, J. A.; Vogt, T. *Chem. Mater.* **1995**, *7*, 75−83.

(54) Wagner, C. D.; Passoja, D. E.; Hillery, H. F.; Kinisky, T. G.; Six, H. A.; Jansen, W. T.; Taylor, J. A. *J. Vac. Sci. Technol.* **1982**, *21*, 933−944.

(55) Taylor, J. A. *J. Vac. Sci. Technol.* **1982**, *20*, 751−755.

(56) Popoola, O. O.; Kriven, W. M. *J. Mater. Res.* **1992**, *7*, 1545−1552.

(57) King, B. R.; Patel, H. C.; Gulino, D. A.; Tatarchuk, B. J. *Thin Solid Films* **1990**, *192*, 351−369.

(58) Starr, D. E.; Mendes, F. M. T.; Middeke, J.; Blum, R.-P.; Niehus, H.; Lahav, D.; Guimond, S.; Uhl, A.; Kluener, T.; Schmal, M.; Kuhlenbeck, H.; Shaikhutdinov, S.; Freund, H.-J. *Surf. Sci.* **2005**, *599*, 14−26.

(59) Sharma, P.; Gupta, A.; Rao, K. V.; Owens, F. J.; Sharma, R.; Ahuja, R.; Guillen, J. M. O.; Johansson, V.; Gehring, G. A. *Nat. Mater.* **2003**, *2*, 673−677.

(60) Griffin, K. A.; Pakhomov, A. B.; Wang, C. M.; Heald, S. M.; Krishnan, K. M. *Phys. Rev. Lett.* **2005**, *94*, 157204−157208.

(61) Kim, H.-S.; Bi, L.; Paik, H.; Yang, D.-J.; Park, Y. C.; Dionne, G. F.; Ross, C. A. *Nano Lett.* **2010**, *10*, 597−602.

(62) Nistor, L. C.; Ghica, C.; Kuncser, V.; Pantelica, D.; Grob, J.-J.; Epurescu, G.; Dinescu, M. *J. Phys. D: Appl. Phys.* **2013**, *46*, 065003−065013.

(63) Kim, D. H.; Bi, L.; Jiang, P.; Dionne, G. F.; Ross, C. A. *Phys. Rev. B: Condens. Matter Mater. Phys.* **2011**, *84*, 014416−014425.

(64) Krahl, T.; Stoesser, R.; Kemnitz, E.; Scholz, G.; Feist, M.; Silly, G.; Buzare, J. Y. *Inorg. Chem.* **2003**, *42*, 6474−6483.

(65) Paulis, M.; Martin, M.; Soria, D. B.; Diaz, A.; Odriozola, J. A.; Montes, M. *Appl. Catal., A* **1999**, *180*, 411−420.

(66) Yashima, T.; Hara, N. *J. Catal.* **1972**, *27*, 329−341.

(67) Barzetti, T.; Selli, E.; Moscotti, D.; Forni, L. *J. Chem. Soc., Faraday Trans.* **1996**, *92*, 1401−1407.

(68) Glazumov, V. P.; Odinokov, S. E. *Spectrochim. Acta, Part A* **1982**, *38*, 399−408.

(69) Maurer, S. M.; Ko, E. I. *J. Catal.* **1992**, *135*, 125−134.

(70) Jehng, J.-M.; Wachs, I. E. *Catal. Today* **1990**, *8*, 37−46.

(71) Jehng, J.-M.; Wachs, I. E. *J. Phys. Chem.* **1991**, *95*, 7373−7379.

(72) Corma, A. *Chem. Rev.* **1995**, *95*, 559−614.

(73) Rosenthal, D. J.; White, M. G.; Parks, G. D. *AIChE J.* **1987**, *33*, 336−340.

(74) Datka, J.; Turek, A. M.; Jehng, J. M.; Wachs, I. E. *J. Catal.* **1992**, *135*, 186−199.

(75) Matulewicz, E. R. A.; Kerkhof, F. P. J. M.; Moulijn, J. A.; Reitsma, H. J. *J. Colloid Interface Sci.* **1980**, *77*, 110−119.

(76) Hughes, T. R.; White, H. M. *J. Phys. Chem.* **1967**, *71*, 2192−2201.

(77) Emeis, C. A. *J. Catal.* **1993**, *141*, 347−354.

(78) Makarova, M. A.; Karim, K.; Dwyer, J. *Microporous Mater.* **1995**, *4*, 243−246.

(79) Khabtou, S.; Chevreau, T.; Lavalley, J. C. *Microporous Mater.* **1994**, *3*, 133−148.

(80) Funaioli, T.; Marchetti, F.; Pampaloni, G.; Zacchini, S. *Dalton Trans.* **2013**, *42*, 14168−14177.

(81) Krahl, T.; Vimont, A.; Eltanany, G.; Daturi, M.; Kemnitz, E. *J. Phys. Chem. C* **2007**, *111*, 18317−18325.

(82) de Clippel, F.; Dusselier, M.; Van Rompaey, R.; Vanelderen, P.; Dijkmans, J.; Makshina, E.; Giebeler, L.; Oswald, S.; Baron, G. V.; Denayer, J. F. M.; Pescarmona, P. P.; Jacobs, P. A.; Sels, B. F. *J. Am. Chem. Soc.* **2012**, *134*, 10089−10101.

(83) Holm, M. S.; Saravanamurugan, S.; Taarning, E. *Science* **2010**, *328*, 602−605.

(84) Rivalier, P.; Duhamet, J.; Moreau, C.; Durand, R. *Catal. Today* **1995**, *24*, 165−171.

(85) Roman-Leshkov, Y.; Davis, M. E. *ACS Catal.* **2011**, *1*, 1566−1580.

(86) West, R. M.; Holm, M. S.; Saravanamurugan, S.; Xiong, J.; Beversdorf, Z.; Taarning, E.; Christensen, C. H. *J. Catal.* **2010**, *269*, 122−130.

(87) Carniti, P.; Gervasini, A.; Biella, S.; Auroux, A. *Chem. Mater.* **2005**, *17*, 6128−6136.

(88) Carniti, P.; Gervasini, A.; Marzo, M. *Catal. Today* **2010**, *152*, 42−72.

(89) Chambon, F.; Rataboul, F.; Pinel, C.; Cabiac, A.; Guillon, E.; Essayem, N. *Appl. Catal., B* **2011**, *105*, 171−181.

(90) Liu, Z.; Li, W.; Pan, C.; Chen, P.; Lou, H.; Zheng, X. *Catal. Commun.* **2011**, *15*, 82−87.